Journal of Chromatography A, 1218 (2011) 4167–4178

Contents lists available at ScienceDirect

Journal of Chromatography A

journal homepage: www.elsevier.com/locate/chroma

Coupling asymmetric flow-field flow fractionation and fluorescence parallel factor analysis reveals stratification of dissolved organic matter in a drinking water reservoir

Ashley D. Pifer, Daniel R. Miskin, Sarah L. Cousins, Julian L. Fairey*

Department of Civil Engineering, University of Arkansas, 4190 Bell Engineering Center, Fayetteville, AR 72701, USA

ARTICLE INFO

Article history:
Available online 21 December 2010

Keywords:
Diffusion coefficient
Polystyrene sulfonate salt
PARAFAC
Dissolved organic matter stratification
Disinfection byproduct precursors

ABSTRACT

Using asymmetrical flow field-flow fractionation (AF4) and fluorescence parallel factor analysis (PARAFAC), we showed physicochemical properties of chromophoric dissolved organic matter (CDOM) in the Beaver Lake Reservoir (Lowell, AR) were stratified by depth. Sampling was performed at a drinking water intake structure from May to July 2010 at three depths (3-, 10-, and 18-m) below the water surface. AF4-fractograms showed that the CDOM had diffusion coefficient peak maximums between 3.5 and 2.8×10^{-6} cm^2 s^{-1}, which corresponded to a molecular weight range of 680–1950 Da and a size of 1.6–2.5 nm. Fluorescence excitation–emission matrices of whole water samples and AF4-generated fractions were decomposed with a PARAFAC model into five principal components. For the whole water samples, the average total maximum fluorescence was highest for the 10-m depth samples and lowest (about 40% less) for 18-m depth samples. While humic-like fluorophores comprised the majority of the total fluorescence at each depth, a protein-like fluorophore was in the least abundance at the 10-m depth, indicating stratification of both total fluorescence and the type of fluorophores. The results present a powerful approach to investigate CDOM properties and can be extended to investigate CDOM reactivity, with particular applications in areas such as disinfection byproduct formation and control and evaluating changes in drinking water source quality driven by climate change.

1. Introduction

In aqueous systems, the term dissolved organic matter (DOM) is used to refer to mixtures of molecules comprised mainly of organic carbon, present in ground and surface waters at low milligram as carbon per liter (mg C L^{-1}) levels. DOM controls geochemical processes, affecting transport, speciation, and bioavailability of trace elements [1], serves as a carbon substrate for the growth of biofilms in water distribution systems [2], and reacts with drinking water disinfectants to form disinfection byproducts, DBPs [3]. The formation of DBPs in treated drinking waters is a public health issue, as many DBPs are regulated because they are suspected human carcinogens. Aquatic DOM is derived from terrestrial and aquatic sources, and can undergo biotic (e.g., microbial) and abiotic (e.g., photolysis) transformations, and, as such, exists as a dynamic carbon pool, the properties of which can vary temporally and spatially [4]. Because of its importance in aquatic systems, detailed DOM characterization techniques are needed to understand its fate in the environment and to develop strategies to minimize its deleterious effects in engineered treatment processes.

Because of the physical and chemical diversity that exists within the aquatic DOM pool, researchers have attempted to isolate various DOM fractions of like size and/or similar chemical composition. Commonly used physicochemical separations include resin adsorption techniques [5,6], liquid chromatography [7], alum coagulation and activated carbon adsorption [8], ultrafiltration [6,9], and flow field-flow fractionation (FlFFF) [10–13]. Once a given DOM fraction has been separated, various analytical techniques are often applied with improved resolution, such as ultraviolet (UV) spectroscopy [7,14,15], measurement of dissolved organic carbon (DOC) [16], inductively coupled plasma mass spectrometry (ICP-MS) [7,17], and fluorescence spectroscopy [18,19]. A well known yet often overlooked aspect of UV and fluorescence spectroscopy, is that these techniques are only sensitive to the chromophoric DOM (CDOM)-the fraction of the DOM pool that absorbs light or imparts color to natural waters.

Using DOM isolated and concentrated by resin adsorption techniques, Cabaniss et al. [20] showed that DOM size affects proton and metals binding, partitioning of organic contaminants, and coagulation and adsorption processes. Other researchers found that the low molecular weight DOM fraction (<10 kDa) was the principal

* Corresponding author. Tel.: +1 479 575 4023.
E-mail address: julianf@uark.edu (J.L. Fairey).

0021-9673/$ – see front matter © 2010 Elsevier B.V. All rights reserved.
doi:10.1016/j.chroma.2010.12.039

component of the total DOM pool [17], and that hydrophilic DOM fractions were linked with formation of nitrogenous DBPs [5]. Despite these potentially valuable insights, previous DOM characterization methods have serious drawbacks. For example, resin adsorption techniques often require DOM pre-concentration [19], perturbations in acid/base chemistry, and employ interactions with a stationary resin phase, all of which can introduce artifacts that bias the DOM sample in varying and often unknown ways [21]. Similarly, contact with a stationary phase is a concern in liquid chromatography separations. While DOM isolation by alum coagulation does not require acid/base perturbations, this technique suffers from inadequate separation of hydrophilic elements [8]. Likewise, ultrafiltration (UF) does not perturb solution chemistry, but the resultant DOM separations often overlap with one another despite distinct membrane cutoffs [22], and further, UF-separated DOM size distributions are erroneously discontinuous in nature [15]. Coupling these various separation methods with ICP-MS, UV spectroscopy, DOC measurements, or combinations thereof (e.g., specific UV absorbance, SUVA), can yield interesting insights, however, it is generally unknown how the results from studies with DOM isolates relate to their unperturbed natural source waters.

Symmetrical FlFFF and asymmetrical FlFFF (AF4) have been used to separate and characterize DOM in natural water samples [12,14] without need for DOM pre-concentration, interaction with a stationary phase, or perturbations of solution chemistry. Both FlFFF techniques provide physical separation of DOM in a ribbon-like channel, but differ in the nature of the applied flow field. The reader is directed to discussions in Ref. [23] for an in-depth comparison of the two FlFFF techniques. AF4 is a newer technology and has several practical advantages over its symmetric counterpart, namely simpler channel construction and a transparent front plate in which the focusing band position can be visualized (when a colored dye is injected) and measured precisely [24]. AF4 separates colloids, macromolecules, and particles from 1-nm to 100-μm in size on the basis of diffusivity [25]. Reported sample injection sizes vary from 5-μL to 250-mL [10,14,26,27], depending on the intended application. In FlFFF, shear forces that drive the sample separation within the channel are low [10], which prevents breakup of DOM aggregates and, as such, FlFFF data can be used to determine the hydrodynamic diameter distribution of DOM mixtures [28]. While FlFFF has some drawbacks (e.g., the inability to precisely determine DOM molecular weight due to the difficulty in finding appropriate standards), these are relatively minor when weighed against the many benefits over traditional DOM separation techniques.

To elucidate important physicochemical properties, FlFFF is often coupled with various analytical detectors. For instance, Floge and Wells [12] coupled FlFFF with UV_{254} to study the rapid cycling of marine colloids in coastal waters; similarly, Alasonati et al. [14] reported substantial spatial variability of DOM in Amazonian basin waters with the aid of a multi-angle light scattering detector. However, fluorescence spectroscopy is arguably the most useful and widely applied detector for DOM studies. Fluorescence measurements consist of two spectra – excitation and emission – that are plotted against one another to yield an excitation–emission matrix (or EEM). Fluorescence EEMs have been used in a variety of applications. For example, Coble [29] showed that marine and terrestrial DOM had distinct fluorescence signatures and identified EEM regions with humic-like and protein-like fluorophores. Similarly, Hall and Kenny [30] showed fluorophores can be used to identify the origin of a water sample in their study of ballast waters from shipping vessels. Other researchers have analyzed changes in fluorescence EEMs upon oxidation with drinking water disinfectants. For instance, Johnstone and Miller [31] correlated changes in fluorescence EEMs with formation of specific DBPs. Recently, fluorescence has been coupled with FlFFF. Notably, Stolpe et al. [15] used FlFFF and fluorescence to characterize colloidal DOM mass transport of trace elements. Additionally, Boehme and Wells [18] showed that the protein-like EEM signature of estuarine DOM samples was associated with the smallest (1–5 kDa) DOM size fraction. However, interpretation of fluorescence data presents analytical challenges due to the presence of water scattering regions, quenching, and instrument noise [32]. Fluorophores have often been identified by ad hoc "peak picking" methods (e.g., [33]) and calculation of various fluorescence indexes (e.g., [34]), but these techniques have proved to have serious limitations [35]. To help address these concerns, parallel factor analysis (PARAFAC), a statistical algorithm, has been developed and successfully used to decompose an array of at least 30 fluorescence EEMs [30,32,36] into several (generally less than 10) principal components. The reader is referred to the seminal work of Bro's group (e.g., [32,37]) for detailed descriptions of PARAFAC theory and its applications to DOM analyses.

Here, AF4 was coupled with fluorescence PARAFAC analyses to elucidate physicochemical properties of CDOM in unperturbed freshwaters, sampled weekly at three depths from a drinking water treatment plant reservoir in Lowell, AR, between May and July 2010. AF4-UV_{254} was used to determine the diffusion coefficient, molecular weight, and size distributions of CDOM and separate it into three distinct fractions. Fluorescence EEMs were measured for whole water samples and AF4-generated fractions, which were decomposed with the PARAFAC model into five principal components. This novel coupling of AF4-UV_{254} and fluorescence PARAFAC analyses revealed that CDOM properties in the reservoir were stratified by depth which may have implications on strategies that drinking water treatment plants use to help limit the formation of DBPs.

2. Materials and methods

2.1. Site description

Water samples were collected from the Beaver Lake Reservoir, which is located on the White River in northwest Arkansas and serves as the main drinking water source for the more than 300,000 customers of the Beaver Water District (BWD). The reservoir has a surface area of 103-km^2, an average depth of 18-m, and an average hydraulic retention time of 1.5-years [38]. The hydraulic catchment area encompasses 310,000-ha of mostly forest and agricultural lands with primary inflows from the White River, Richland Creek, War Eagle Creek, and Brush Creek. The BWD's intake structure (the sampling site) is located in a transitional zone of the reservoir, where conditions vary from mesotrophic to eutrophic. However, with increased urbanization and poultry production in the area, conditions may become increasingly eutrophic. Increases in nutrient loadings have stimulated growth of aquatic plant life, and hence have the potential to drive changes in the concentration and reactivity of the DOM in the reservoir.

2.2. Sample handling and collection

Beaver Lake water (BLW) samples were collected weekly over eight weeks from May to July 2010 at the BWD's intake structure. Sampling was performed with a 6-L Van Dorn bottle (Wildco, Model 1960-H65, Yulee, FL) tethered to a 30-m rope for collection of water at three depths (3-, 10-, 18-m) below the water surface. Samples were transferred to pre-rinsed (Milli-Q water) 9-L HDPE carboys, capped, transported to the Water Research Laboratory at the University of Arkansas, and stored in the dark at 4 °C until use. Prior to AF4 and fluorescence analyses, each water sample was filtered through a 1 μm nominal pore size glass fiber filter (GFF), which was pre-combusted (at 400 °C for 30 min) and pre-rinsed with 1-L of Milli-Q water. The sample filtrate was stored in the dark at 4 °C

in 250-mL amber glass bottles capped with PTFE-lined lids. Prior to all analyses, samples were warmed to room temperature.

Glassware was soaked in a solution of tap water and Alconox detergent, scrubbed thoroughly, rinsed with copious amounts of Milli-Q water, and baked in a muffle furnace at 400 °C for 30 min. Volumetric flasks and plastic-ware were prepared similarly, but instead of baking, were dried at room temperature and 40 °C, respectively.

2.3. Water quality tests

All water for aqueous phase preparations was made using a Millipore Integral 3 (Billerica, MA) Milli-Q water system (18.2 MΩ-cm) and ACS-grade chemical reagents. The pH of the sample waters was measured using an Orion 8272 pH electrode (Thermo Orion, Waltham, MA) calibrated with pH standards of 4, 7, and 10 and connected to an Accumet XL60 dual channel pH/Ion/Conductivity meter. Alkalinity was measured following Standard Methods 2320B [39], in which waters were titrated to pH 4.5 with 0.1 N HCl. Turbidity was measured using a HF Scientific DRT-100 turbidimeter (Fort Myers, FL), which was calibrated (0.5–50 NTU) with standards made by dilutions of a 4000 mg L^{-1} stock formazin suspension (Ricca Chemical Company, Arlington, TX). Conductivity was measured with an Accumet four-cell conductivity probe. UV_{254} was measured on a Shimadzu UV-Vis 2450 (Kyoto, Japan) spectrophotometer using a 1-cm path length low volume quartz cell. Samples for UV analyses were filtered with pre-combusted and pre-rinsed GFFs. Following the same filtration protocol, dissolved organic carbon (DOC) was measured in triplicate with a Shimadzu TOC-V_{CSH} TOC analyzer (Kyoto, Japan) equipped with an auto-sampler and TOC-Control V acquisition software. Specific ultraviolet absorbance (SUVA) was calculated by dividing the UV_{254} by the product of the DOC and UV cell path length.

Total ammonia (the sum of NH_3 and NH_4^+) was measured using an ammonia electrode (Thermo Orion 9512, Waltham, MA) connected to the Accumet XL60 meter. To calibrate the ammonia probe, a 1000 mg L^{-1}-N stock ammonium chloride solution was prepared following Standard Methods 4500-NH_3 D and diluted to make standards between 0.03 and 10 mg L^{-1}-N ($R^2 = 1$, $n = 19$). Nitrate was measured on filtered water samples using Hach HR NitraVer 5 (Hach Company, Loveland, CO) powder pillows with the spectrophotometer at 392 nm. Nitrate standards were prepared following Standard Methods 4500-NO_3^- C using 10 mg L^{-1} KNO_3 solution (JT Baker, Phillipsburg, NJ). Similarly, nitrite was measured on filtered water samples using Hach LR Nitrite powder pillows at 548 nm. Nitrite standards were prepared following Standard Methods 4500 NO_2-B using $NaNO_2$ (MP Biomedicals Inc., Solon, OH). Lastly, iron was determined as total iron using Hach FerroVer Iron reagent and measured at 540 nm. Iron standards were made with $FeCl_3 \cdot 6H_2O$ at Fe^{3+} concentrations between 0.2 and 3.5-mg Fe L^{-1}.

2.4. Asymmetric flow-field flow fractionation

An AF2000-MT asymmetrical flow field-flow fractionation (AF4) system from Postnova Analytics (Salt Lake City, UT) was used to characterize the physicochemical properties of the BLW CDOM. The AF4 system consisted of four pumps, a separation channel, 1.0–1.5-m of black PEEK tubing (to generate adequate system pressure, 5–18 bar), an inline UV detector and fraction collector, and an offline fluorescence excitation–emission detector. The pumps were used to introduce carrier fluid (referred to herein as "eluent") and the sample to the separation channel and create the flow-field for macromolecular separation. The AF4 pumps were controlled by Postnova Software (AF2000 Control v.1.1.0.25) and the detectors and fraction collector were controlled by Agilent Chemstation for LC Systems (rev. B.04.01 SP1). The eluent consisted of 1-mM NaCl in Milli-Q water, and was chosen to match the conductivity of the BLW samples (~160 μS cm^{-1}). The eluent was passed through an inline vacuum degasser (PN7520) before being pumped through the system to prevent formation of bubbles within the system. Two HPLC pumps (PN1130) provided independent control of the tip and focus flow rates. A syringe pump was used for the cross-flow, which drew the non-macromolecular fluid through the channel membrane to the waste and controlled the magnitude of the applied flow-field. Another syringe pump, the slot pump (PN1610), was used during elution to concentrate the sample passing through the UV detector [27] and fraction collector.

Table 1
Asymmetric flow-field flow fractionation pump flow rates.

Phase	Flow rates (mL min^{-1})			
	Tip	Focus	Cross-flow	Slot
Injection	2.0	2.3	4.0	0.0
Focusing	0.2	4.3	4.0	0.2
Elution	4.5	0.0	4.0	0.2
Rinsing	5.0	0.0	0.0	0.0

The separation channel is the heart of the AF4 system, a schematic of which is shown in Figure SM1. The tip-to-tip channel length was 27.4 cm, with an effective channel length (L_{eff}), the distance from the focusing band to the channel outlet, of 24.5 cm. The channel breadth geometry tapered symmetrically from a maximum of 2.0 cm (b_0) to 0.7 cm (b_L) at the outlet. The nominal Mylar spacer thickness was 500 μm, but the actual channel thickness was 410 μm, which was calculated using the AF4-elution time (t_r = 15 min) of the bovine serum albumin monomer in 100 mM NaCl and Eq. (1) with a diffusion coefficient of 6.7×10^{-7} cm^2 s^{-1} [40]. Polyethersulfone (PES) channel membranes with a 300-Da molecular weight cut-off (Postnova Analytics) were used throughout this study.

An AF4 sample run consists of four phases: (1) injection, (2) focusing, (3) elution, and (4) rinsing. Individual pump flow rates varied between phases and shown in Table 1. Throughout Phases 1–3, the detector flow rate was held constant at 0.3 mL min^{-1}; in Phase 4, the flow passed through the purge line to flush the system.

Ten-milliliter samples were injected into the AF4 channel using a bubble trap (Postnova Analytics). This injection volume was chosen to balance adequate UV detection with minimization of sample loss through the channel membrane during the injection and focusing steps [28]. The tip pump flow was plumbed through the bubble trap and carried the sample into the channel over 6 min. Concurrently, eluent from the focus pump was supplied to the channel 18.5-cm from the inlet (L_{FP} in Fig. SM1), and a portion of this flow traveled toward the channel inlet to keep sample macromolecules in the channel. Eluent exited the channel during the injection step through the channel membrane by the action of the cross-flow pump, which acted perpendicular to the long dimension of the channel. Sample injection was followed by 6 min of focusing, designed to focus the sample into a uniform band near the channel inlet (at z' in Figure SM1). Next, in the transition phase, the focus pump flow was decreased to zero as the tip pump ramped up to maintain the total flow over 1-min, followed by the elution step and 5-min of rinsing.

Following the AF4 channel outlet, the fractionated sample flowed to an inline UV-diode array detector (Agilent Technologies, G1315D), which collected UV data from 200 to 800 nm in 1 nm increments every 2-s during the 20-min sample elution. UV_{254} was used to calculate the diffusion coefficient distributions of the samples. Following the UV detector, the samples were physically separated using a fraction collector (Agilent Technologies, Model 1364C). Three equal-volume fractions (denoted F1, F2, and F3 herein) were collected in 2-mL pre-washed vials beginning at

1-min elution and ending at 8-min elution. UV_{254} time series fractograms were baseline corrected using the FFF Analysis software (Postnova Analytics v. 2.03A). The fractogram data were used to determine the maximum UV_{254} peak heights (MaxUV) and area under the curves (PeakArea), which was calculated using numerical integration with Simpson's method in the freeware program R (v. 2.10.1). Calculation of the diffusion coefficient from the time-series data is detailed in Section 3.

2.5. Fluorescence

Fluorescence excitation–emission matrices (EEMs) were collected with a dual monochromator fluorescence detector (Agilent Technologies, Model G1321A) equipped with a static sample cuvette at 1-nm increments for excitation wavelengths between 200 and 400 nm and emission wavelengths between 270 and 600 nm. The fluorescence cuvette was flushed thoroughly with Milli-Q water between scans to prevent carryover and sample contamination. All scans were corrected for first- and second-order Rayleigh and Raman water scattering using a MATLAB® *Cleanscan* program developed by Zepp et al. [41]. *Cleanscan* was applied to each EEM and removed water scattering peaks and replaced them with a surface created by a 3-dimensional Delauney interpolation algorithm. The areas of the EEMs over which *Cleanscan* was invoked are shown in Fig. SM2.

Rather than relying on the peak picking methods used in previous works (e.g., Coble [29]), fluorescence PARAFAC modeling was used to identify the principal fluorophores and their maximum intensities, F_{MAX}, for all scatter-corrected EEMs. The EEMs were analyzed using MATLAB® functions contained in the *DOM-Fluor toolbox* (available for download at http://www.models.life.ku.dk/algorithms). First, the fluorescence data was imported into MATLAB® as a collection of individual EEMs, stacked into a 3-dimensional structure using the function *Loading data for DOMfluor*. PARAFAC models require the removal of outliers because they can disproportionately influence the overall model output. Outliers can be the results of measurement error (e.g., sample movement within the cuvette leading to "wrinkles" in the EEM) or can be atypical samples. Such samples were identified visually and by running the function *OutlierTest*. This test calculated and plotted leverages for each EEM, and identified those considered as possible outliers based on high leverage values relative to the other samples. For example, sample numbers 38, 81, and 100 in Fig. SM3 were identified as likely outliers. In cases where EEMs were deemed to have both measurement errors and high leverages, these samples were removed from the PARAFAC dataset. Next, the outlier program was used on the reduced dataset, and additional samples were identified as requiring further investigation after an initial estimate of the proper number of PARAFAC components. The *Split-half analysis* tool was used for this step. The function, *SplitData*, divided the EEM dataset into two pairs of halves. These halves were used in the functions *SplitHalfAnalysis* and *SplitHalfValidation* which compared the shape of components derived from each half of the dataset with the other half's components' shapes. When component shapes from each half were identical, the corresponding model and number of PARAFAC components was considered robust [37]. Fig. SM4 shows an example of one unvalidated (the 4-component) and two validated (the 3- and 5-component) split-half analysis models.

To ensure that all outliers were removed, questionable samples identified by the outlier test were removed from the dataset one by one and split half analysis was repeated. Samples were judged to be outliers if their removal changed the outcome of the split half analysis. This resulted in a total of 87 EEMs in the PARAFAC model. In the case that more than one set of components could be split half validated, the *CompareSpecSSE* function was used to plot the sum of squared error (SSE) versus excitation and emission wavelengths [42]. The SSE for excitation and emission were normalized by the sum of squares for excitation and emission and were plotted to give a visual indication of the level of residual fluorescence compared to the measured fluorescence signal (Fig. SM5). This plot showed that the 5-component model was superior to the 3-component model. As a final check, plots of loadings versus excitation and emission wavelengths for each PARAFAC component were generated and visually inspected. Stedmon and Bro [37] suggested that these plots ideally show emission loadings with a single peak and excitation and emission loadings slightly overlapping. Discussion of these results is contained in Section 4.3.

Following the technique used by Fellman et al. [43], the percent relative contribution of each PARAFAC component was determined using F_{MAX} values for each PARAFAC component for all 87 EEMs. For a given EEM, F_{MAX} for each component was divided by the sum of F_{MAX} for all the components (F_{MAX_TOT}). For the whole water samples and AF4-generated fractions, these quotients were averaged for each sample depth (3-, 10-, 18-m) and converted to a percentage. This procedure simplified the interpretation of the PARAFAC data, and conveys the relative contribution of the PARAFAC components at a given sample depth for each water fraction.

3. Calculation

The diffusion coefficient, D_f (in $cm^2\ s^{-1}$) for the AF4-fractograms was calculated using Eq. (1):

$$D_f = \lambda \frac{V_C w^2}{V^0} \tag{1}$$

In Eq. (1), λ denotes the unitless retention parameter, V_C is the cross-flow rate ($4.0\ mL\ min^{-1}$), w is the experimentally determined channel thickness (0.041 cm, Section 2.3), and V^0 is the channel void volume, calculated by the product of channel thickness and the effective channel area. The effective channel area, A_{eff}, was calculated as the channel area downstream of the sample focus band, $b_{z'}$, which was located 2.9 cm downstream of the channel inlet, as indicated in the channel schematic (Fig. SM1). Using similar triangles, A_{eff} was calculated to be $32\ cm^2$. The effective channel area was also used to find α, a term used in the calculation of the void time, t^0, by Eq. (2).

$$\alpha = 1 - \frac{((b_0 z' - b_L)(z')^2/2L_{eff}) - y}{A_{eff}} \tag{2}$$

In Eq. (2), b_0 is the maximum channel width, b_L is the width of the narrowest part of the trapezoidal channel section, z' is the distance from the channel inlet to the focusing band, L_{eff} is the effective channel length, and y is the channel area lost by the tapered channel ($3.4\ cm^2$). The void time, t^0, in seconds was then calculated with Eq. (3).

$$t^0 = \frac{V^0}{V_c} \ln\left(1 + \alpha \frac{V_c}{V_{OUT}}\right) \tag{3}$$

In Eq. (3), V_{OUT} is the volumetric flow rate of the channel outlet ($0.5\ mL\ min^{-1}$). The value of t^0 was divided by the time series data to determine the unitless retention ratio values, R, shown in Eq. (4), which is also equal to six times the retention parameter values, λ [23].

$$\frac{t^0}{t_r} = R = 6\lambda \tag{4}$$

Values of λ were then used in Eq. (1) to determine the diffusion coefficient distribution. The hydrodynamic diameter, d_h, of the DOM was approximated from the molecular weight (MW) using Eq. (5), similar to the procedure used by Howe and Clark [44].

$$d_k = 0.009(\mathrm{MW})^{0.44} \tag{5}$$

Table 2
Water quality parameters for the Beaver Lake Water (BLW) samples.

Date	Depth (m)	pH	Turbidity (NTU)	Conductivity ($\mu S\,cm^{-1}$)	Alkalinity ($mg\,L^{-1}$-$CaCO_3$)	Ammonia ($mg\,L^{-1}$-N)	Nitrate ($mg\,L^{-1}$-N)	Nitrite ($\mu g\,L^{-1}$-N)	DOC ($mg\,L^{-1}$-C)	SUVA ($L\,mg^{-1}\,m^{-1}$)
5/27/10	3	8.0	4	231	62	0.20	0.52	166.9	3.2	2.8
	10	8.1	18	159	62	0.05	0.95	10.0	2.2	5.6
	18	8.1	7	164	60	0.46	0.86	1.3	1.3	3.0
6/15/10	3	8.2	1	158	62	0.29	0.38	12.4	2.1	2.6
	10	7.8	8	156	59	0.07	1.08	8.4	2.1	4.9
	18	7.6	9	171	63	0.04	1.04	5.2	1.7	2.8
6/22/10	3	9.1	2	153	67	0.16	0.07	11.6	2.3	2.3
	10	7.7	13	135	52	0.04	1.03	9.6	8.2	2.1
	18	7.8	9	167	60	0.04	1.08	2.3	1.5	3.1
6/29/10	3	9.3	2	141	57	0.05	BD	5.4	2.6	2.1
	10	7.7	15	137	54	0.02	1.01	9.6	2.7	5.1
	18	7.8	10	177	61	0.05	1.03	4.7	13.2	0.4
7/08/10	3	8.9	2	150	59	0.07	0.22	5.3	2.4	2.1
	10	7.6	18	147	58	0.01	0.98	4.5	24.7	0.4
	18	7.7	20	171	62	0.03	1.05	3.7	8.2	0.7
7/13/10	3	8.7	3	148	58	0.04	0.14	4.8	2.2	2.2
	10	7.7	21	173	58	0.05	0.94	5.6	2.5	4.5
	18	7.7	21	169	63	0.03	0.99	4.8	1.7	3.5
7/20/10	3	9.2	1	152	62	0.04	0.16	7.6	10.0	0.4
	10	7.7	8	150	61	0.16	0.53	5.5	2.4	4.5
	18	7.6	13	172	66	0.13	1.01	7.2	2.6	2.8
7/27/10	3	9.1	2	154	63	0.05	0.11	3.7	2.0	2.0
	10	7.9	15	171	73	0.34	0.26	19.6	2.5	3.6
	18	7.8	15	171	68	0.31	0.53	68.0	2.3	3.8
Mean	NA	8.1	10	162	61	0.11	0.67	16.2	4.4	2.8
Median	NA	7.8	9	159	62	0.05	0.90	5.6	2.4	2.8

BD—below detection; NA—not applicable.

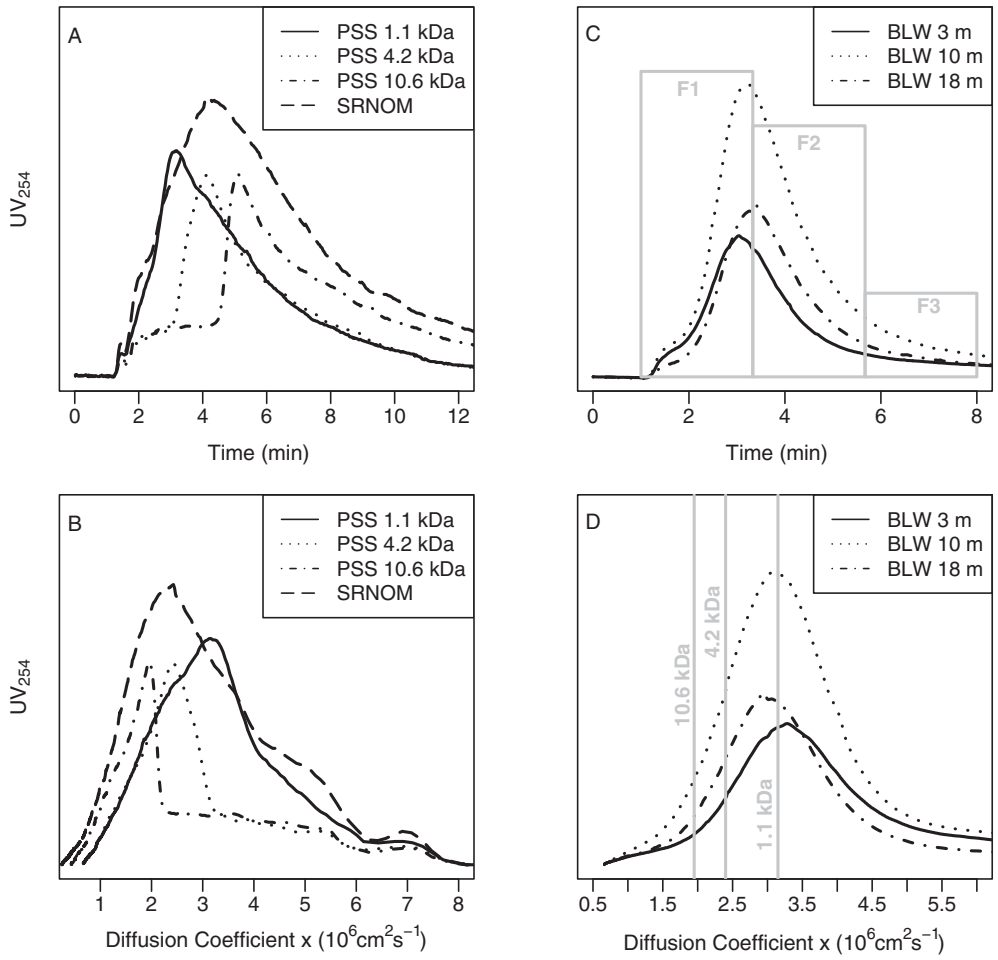

Fig. 1. Asymmetric flow-field flow fractionation (AF4) fractograms of polystyrene sulfonate (PSS) standards and Suwannee River natural organic matter (SRNOM) as a function of time (A) and diffusion coefficient (B). AF4 fractograms of Beaver Lake Water (BLW) sampled on July 8, 2010 at depths of 3-, 10-, and 18-m as a function of time (C) and diffusion coefficient (D). Boxes in (C) represent the three fractions (F1–F3) collected for subsequent fluorescence analyses. Dashed lines in (D) represent the peak maximums of the PSS standards.

4. Results and discussion

4.1. Water quality parameters

The raw water characteristics for the 24 BLW samples are reported in Table 2 along with their mean and median values. All waters had a slightly alkaline pH, low turbidity, and low to moderate alkalinity. Mean and median values were similar for pH (8.1 and 7.8), turbidity (10- and 9-NTU), conductivity (162- and 159-$\mu S\,cm^{-1}$), and alkalinity (61- and 62-$mg\,L^{-1}$-$CaCO_3$), reflecting the tightly bunched nature of these metrics amongst the water samples. Conversely, mean and median values differed for ammonia (0.11- and 0.05-$mg\,L^{-1}$-N), nitrate (0.67- and 0.90-$mg\,L^{-1}$-N), nitrite (16.2- and 5.6-$\mu g\,L^{-1}$-N), and DOC (4.4- and 2.4-$mg\,L^{-1}$-C), indicating these metrics were skewed by a handful of low (for nitrate) and high (for ammonia, nitrite, and DOC) values. Fig. SM6 shows a pair-wise scatter-plot for the water quality parameters. While there were no temporal trends (those with *date*), spatial trends (those with *depth*) were only apparent for pH, turbidity, and nitrate (second column in Fig. SM6). Values for pH were higher at 3-m than at 10- and 18-m; conversely, turbidities were lower at 3-m compared to the 10- and 18-m depths likely because of higher sediment loadings near the bottom of the reservoir.

Total iron was not reported in Table 2 because these values were below 0.33 $mg\,L^{-1}$-Fe, with 22 of the 24 samples below the estimated detection limit (0.20 $mg\,L^{-1}$-Fe) of the Hach FerroVer test. Weishaar et al. [45] evaluated potential interferences of background analytes on UV_{254} and determined that a UV_{254} of 0.01 required 1 $mg\,L^{-1}$-Fe total iron and in excess of 23 $mg\,L^{-1}$-N nitrate. Given the iron and nitrate concentrations in the sample waters were below these thresholds, we concluded that the UV_{254} measurements (for the SUVA calculations and AF4 fractograms) were not impacted by dissolved iron and nitrate.

Interestingly, the four samples with high DOC values (those above 8 $mg\,L^{-1}$ C in Table 2) all had below average alkalinity values (<62 $mg\,L^{-1}$-$CaCO_3$), suggesting the carbonate system controlled the alkalinity of all lake water samples and the diverse groups of weak acids present in the DOM did not contribute significantly to alkalinity. SUVA, calculated as UV_{254} divided by the product of the UV cell path length (0.01-m) and DOC, varied from 0.4- to 5.6-$L\,mg\,C^{-1}\,m^{-1}$. Weishaar et al. [45] showed that SUVA had a strong positive correlation with ^{13}C NMR (a direct measure of DOM aromaticity), but was weakly correlated with trihalomethane formation (a principal group of DBPs), suggesting non-aromatic compounds present in DOM mixtures contributed significantly to DBP formation. Therefore, for the waters in this study, the range of SUVA values suggest a wide array of CDOM aromaticities, but cannot be used to reliably estimate the DBP formation potential.

4.2. AF4-fractograms

In Fig. 1, AF4-fractograms were plotted as a function of elution time (t_r) and diffusion coefficient (D_f). Fig. 1A and B shows the fractograms of 1.1-, 4.2-, and 10.6-kDa polystyrene sulfonate sodium

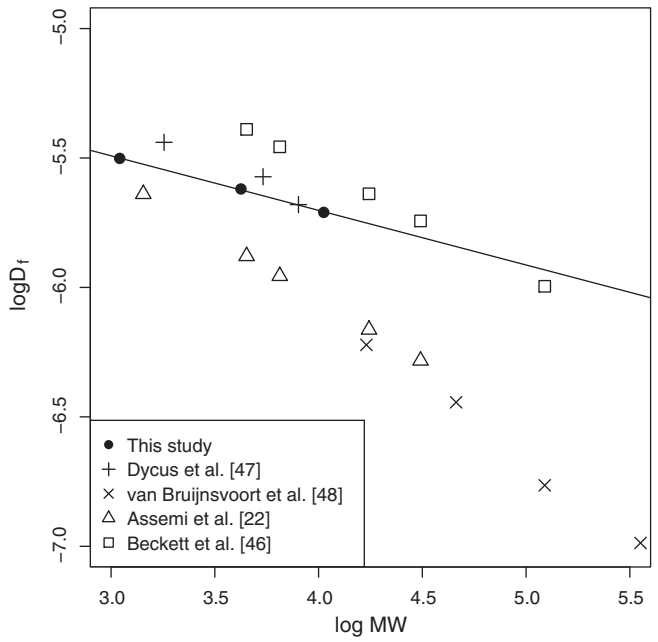

Fig. 2. Diffusion coefficient, D_f, as a function of molecular weight, MW, for the polystyrene sulfonate (PSS) standards and log-linear regression line. Data from the literature is shown for comparative purposes but was not used to generate the regression line.

salt (PSS) standards (ca. 30 mg L^{-1} in 0.001 M NaCl), which other researchers [22,46] have recommended as a molecular weight surrogate for humic substances. For each PSS standard, D_f at the peak maximum was plotted against its molecular weight and compared to PSS data from other research groups [22,46–48] (Fig. 2). These data show that the D_f values determined here were bracketed by those reported in the literature. The spread in these data between research groups (approximately one-half an order of magnitude in log D_f for log MW values less than 4.0) can likely be attributed to different background electrolyte compositions.

The AF4-fractogram of Suwannee River natural organic matter (SRNOM, International Humic Substances Society, Atlanta, GA, Cat. No. 1R101N; ca. 4 mg L^{-1} in 0.001 M NaCl) is also shown in Fig. 1A and B. This peak was broader than those of the PSS standards, with a peak maximum near that of the 4.2 kDa PSS standard (t_r = 4.2 min, Fig. 1A; $D_f = 2.4 \times 10^{-6}$ cm^2 s^{-1}, Fig. 1B) and a "shoulder-like" feature indicating the presence of CDOM smaller than 1.1 kDa PSS (t_r = 2 min, Fig. 1A; $D_f = 5.0 \times 10^{-6}$ cm^2 s^{-1}, Fig. 1B). This broad range of D_f determined here for SRNOM ($\sim$1.0–5.0 $\times 10^{-6}$ cm^2 s^{-1}) was smaller than that reported by Moon et al. [49] of 4.1–5.5 $\times 10^{-6}$ cm^2 s^{-1} (Table 3). However, when coupled with the results of the PSS standards (Fig. 2), it can concluded that the AF4 methods used here produced similar results to those reported by other research groups, for which a variety of preparative and analytical techniques were used.

Fig. 1C and D shows AF4-fractograms for BLW CDOM samples collected on July 8, 2010 at depths of 3-, 10-, and 18-m. The trends shown in Fig. 1D were typical of the other 21 fractograms (Fig. SM7), with BLW CDOM at the 10-m depth having greater UV_{254} peak maximums (with the exception of the first two sampling days) than the samples collected at 3- and 18-m depths. All fractograms had a small, shoulder-like void peak at an elution time of 1.5-min followed by a larger, broad sample peak between 2- and 6-min. The grey boxes in Fig. 1C denote the three fractions (F1–F3) that were collected for subsequent fluorescence analyses (Section 4.3). For the 24 BLW CDOM fractograms, the D_f peak maximum ranged from 3.5- to 2.8 $\times 10^{-6}$ cm^2 s^{-1}. The peak maximums of the three PSS standards were appended as dashed lines in Fig. 1D, and indicate the BLW CDOM was most similar in diffusivity to that of the 1.1-kDa PSS standard. The approximate molecular weight range of the BLW CDOM was calculated by comparison to the PSS data. Here, the log-linear trend line for the three PSS standards (Fig. 2, $R^2 = 1$, $P < 0.02$, slope: −0.21, y-intercept: −4.86) was used with the range of D_f peak maximums (3.5–2.8 $\times 10^{-6}$ cm^2 s^{-1}) to determine the molecular weight of BLW CDOM (680–1950 Da). Using Eq. (5), this corresponded to a size range of 1.6–2.5 nm. The molecular weights and diffusivities for the BLW CDOM were compared to literature-reported values for the various humic substances (Table 3), which, on balance, indicated the results determined here were within the reported ranges of CDOM using a variety of preparative and analytical techniques. Thus, it can be concluded that BLW CDOM was composed primarily of relatively low molecular weight aromatic carbon-containing molecules (680–1950 Da) with diffusivities between 3.5 and 2.8 $\times 10^{-6}$ cm^2 s^{-1}. However, it should be stressed that UV_{254} was used to monitor the AF4-fractrogram output, and as such, non-aromatic containing DOM was not characterized. As such, there is a possibility that colloidal DOM (3000–100,000 Da), much larger than the fraction found here, was also present in the BLW samples, as reported by Howe and Clark [44] in their membrane fouling study, but could not be "seen" by UV_{254}.

The AF4-fractogram data (the UV_{254} peak maximums, MaxUV, and the area under each curve, PeakArea) were compared to select water quality data (DOC and SUVA) as a function of sample date and depth. Fig. 3 shows a pair-wise scatter-plot of these data, which indicated there were no temporal trends (those with *date*). Conversely, trends with sample *depth* were apparent for SUVA, MaxUV and PeakArea (the second column of Fig. 3). As indicated by the trend lines, all these metrics were on balance higher for the 10-m samples compared to the 3- and 18-m samples. Given SUVA is a surrogate for aromatic carbon [45], these results indicate that the nature of the CDOM pool in the Beaver Reservoir was stratified by depth over the 8-week sampling period. The strong linear relationship between MaxUV and PeakArea ($R^2 = 0.97$, $P < 0.001$) indicated that only one of these metrics needed to be determined to adequately describe the AF4-fractogram data; for simplicity, MaxUV was selected for further analyses. For the 24 lake water samples, MaxUV varied from 20 to 85 absorbance units (data not shown) and was uncorrelated with DOC (Fig. 3). However, MaxUV and SUVA had a weak positive correlation (Fig. 3, $R^2 = 0.21$, $P = 0.024$), suggesting that MaxUV would not be a good surrogate of CDOM aromaticity, but may be helpful in assessing CDOM reactivity in DBP studies.

4.3. Fluorescence-PARAFAC analyses

Fluorescence excitation–emission matrices (EEMs) of the 24 whole water samples and 72 AF4-generated fractions were processed as described in Section 2.4. PARAFAC modeling began with the 96 samples, 11 of which were removed based on the protocol detailed in Section 2.4. Split half analyses on the remaining 85 samples showed that three- and five-component models were appropriate for the dataset (Fig. SM4). Fig. SM5 shows the integrated excitation and emission spectra for the sum of squared errors for three- and five-component models and the relative SSE normalized by the total sum of squares. The presence of peaks in these spectra corresponds to regions of the EEMs that are less well described by the model. The results in Fig. SM5 show that a five-component model was superior to the three-component model over the range of excitation and emission wavelengths. For the five-component model, the normalized residual excitation between 200 and 375 nm was less than 1% of the measured signal; similarly, the normalized residual emission between 300 and 525 nm was less than 2%. As such, a 5-component PARAFAC model was selected. However, Component 3 (Fig. SM8) was present in all samples and blanks

Table 3
Literature-reported diffusion coefficients for humic substances.

Sample	Molecular weight (Da)	Diffusion coefficient ($\times 10^6$ cm^2 s^{-1})	Reference
Suwannee River fulvic acid	1340	3.4[a]	[47]
Nordic fulvic acid	2137	3.3[a]	
Nordic humic acid	3264	2.7[a]	
Suwannee stream fulvate	860	4.1	[46]
Suwannee stream humate	1490	3.2	
Trehorningen	2900	2.4[b], 2.6[c]	[52]
Hellerudmyra—May	3900	2.1[b], 2.2[c]	
Hellerudmyra—October	3700	2.2[b], 2.2[c]	
Aurevann	2400	2.6[b], 2.7[c]	
Maridulsvann	2900	2.3[b]	
Birkenes	3500	2.2[b], 2.4[c]	
Humex B	3600	2.2[b], 2.4[c]	
Suwannee River fulvic acid	530–1640	2.2–3.3[a]; 2.4–2.8[b]; 2.4–3.5[d]	[53]
Suwannee River natural organic matter	–	4.1–5.5[a]	[49]
Suwannee River humic acid	–	4.5–5.8[a]	
Suwannee River fulvic acid	–	3.6–4.6[a]	
Nakdong River natural organic matter	1270	5.6[a]	[54]

[a] Flow-field flow fractionation.
[b] Reverse osmosis isolation followed by fluorescence correlation spectroscopy.
[c] Vacuum evaporation isolation followed by fluorescence correlation spectroscopy.
[d] Pulsed field gradient nuclear magnetic resonance (NMR).

(Milli-Q water) at similar intensity (results not shown) and was therefore excluded from further analyses as it was likely a result of instrument noise. Thus, we focus the analysis on Components 1, 2, 4, and 5. These four PARAFAC components and their corresponding component loadings are shown in Fig. 4. The component loadings (Fig. 4, right-side panels) resemble the shape of organic fluorophores described by Stedmon and Bro [37] and contain single emission peaks that slightly overlap the excitation loadings.

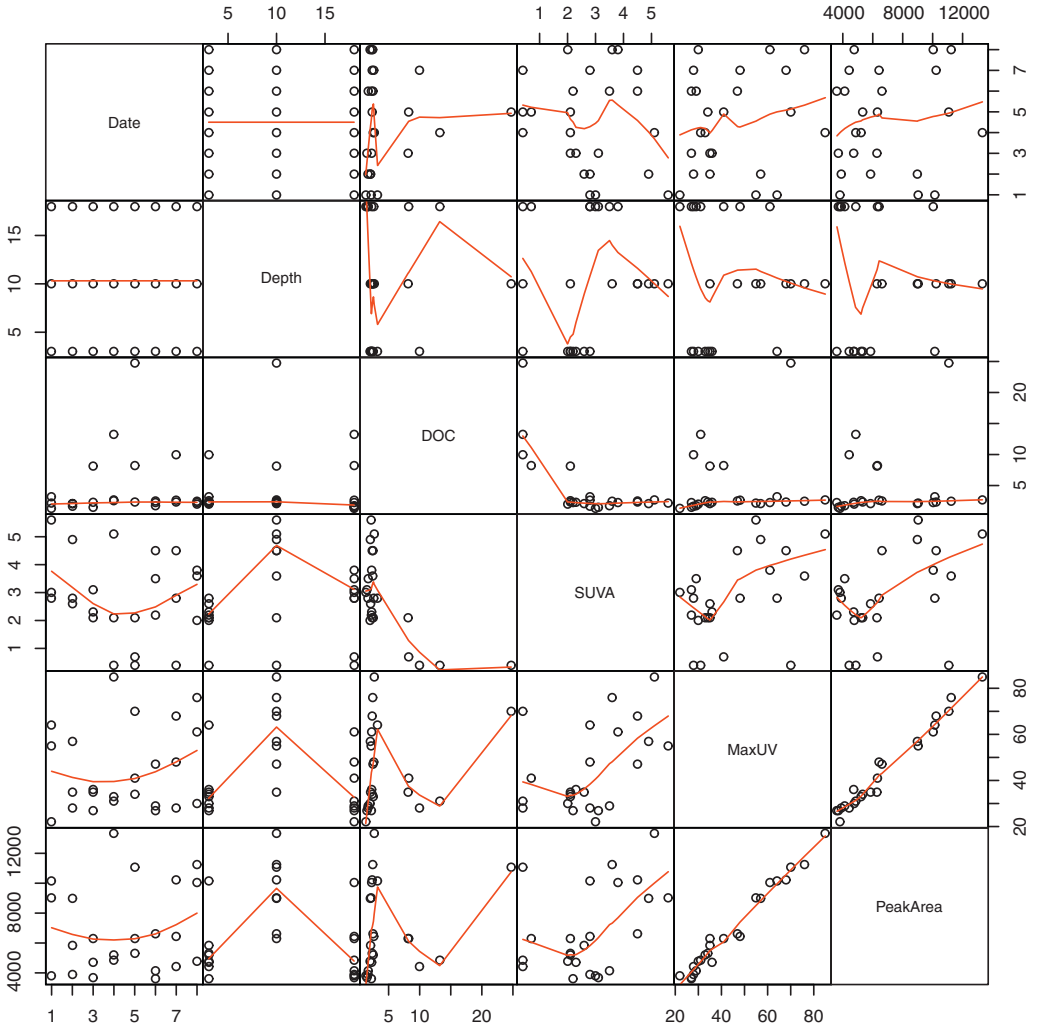

Fig. 3. Pair-wise scatterplot of the asymmetric flow-field flow fractionation (AF4) fractogram data (MaxUV and PeakArea), dissolved organic carbon (DOC), specific ultraviolet absorbance (SUVA), and sample collection date and depth.

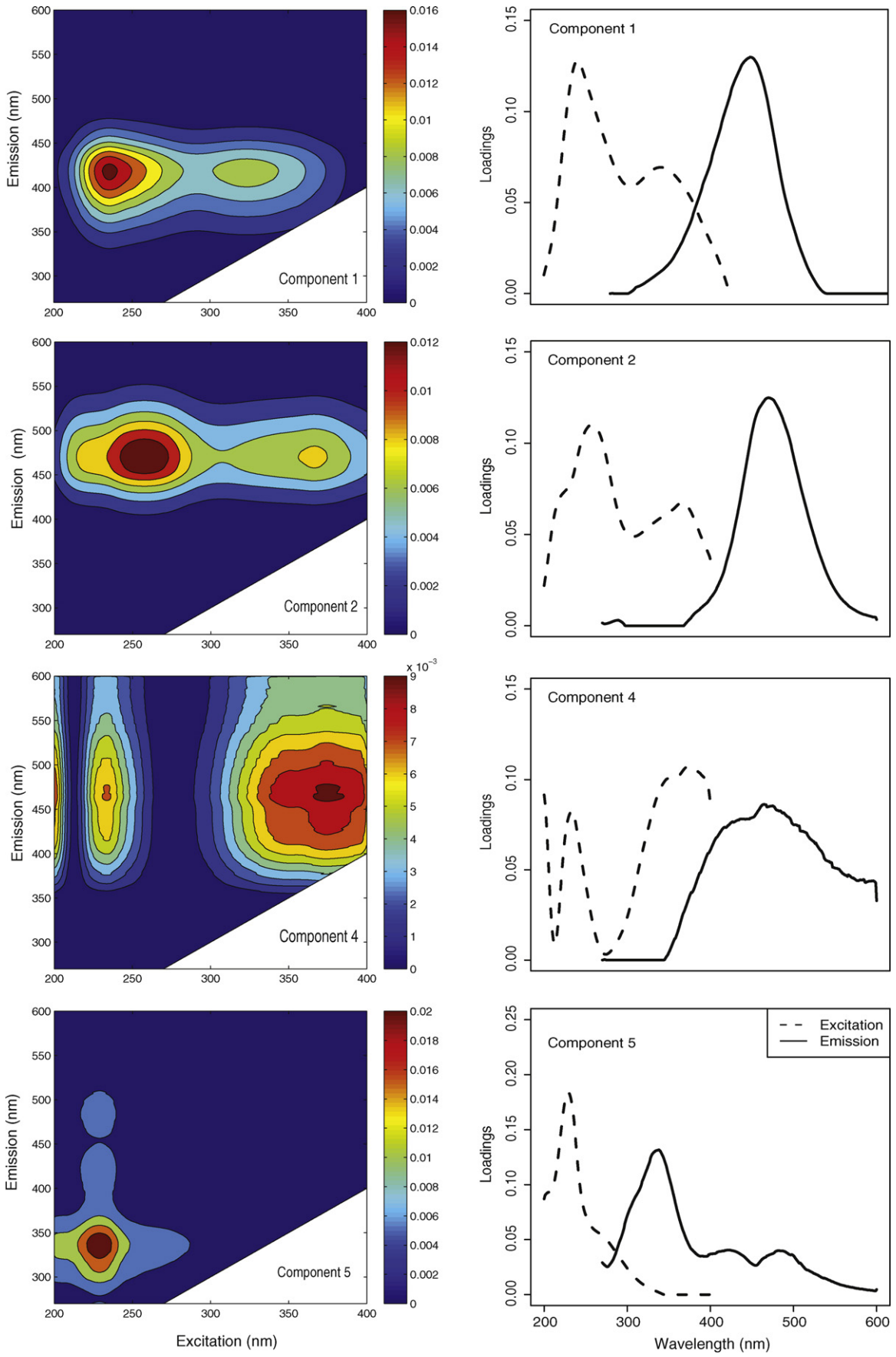

Fig. 4. Fluorescence Components 1, 2, 4, and 5 identified by the PARAFAC model shown as excitation–emission matrices (EEMs) in the left-side panels and their corresponding excitation and emission loadings as a function of wavelength in right-side panels.

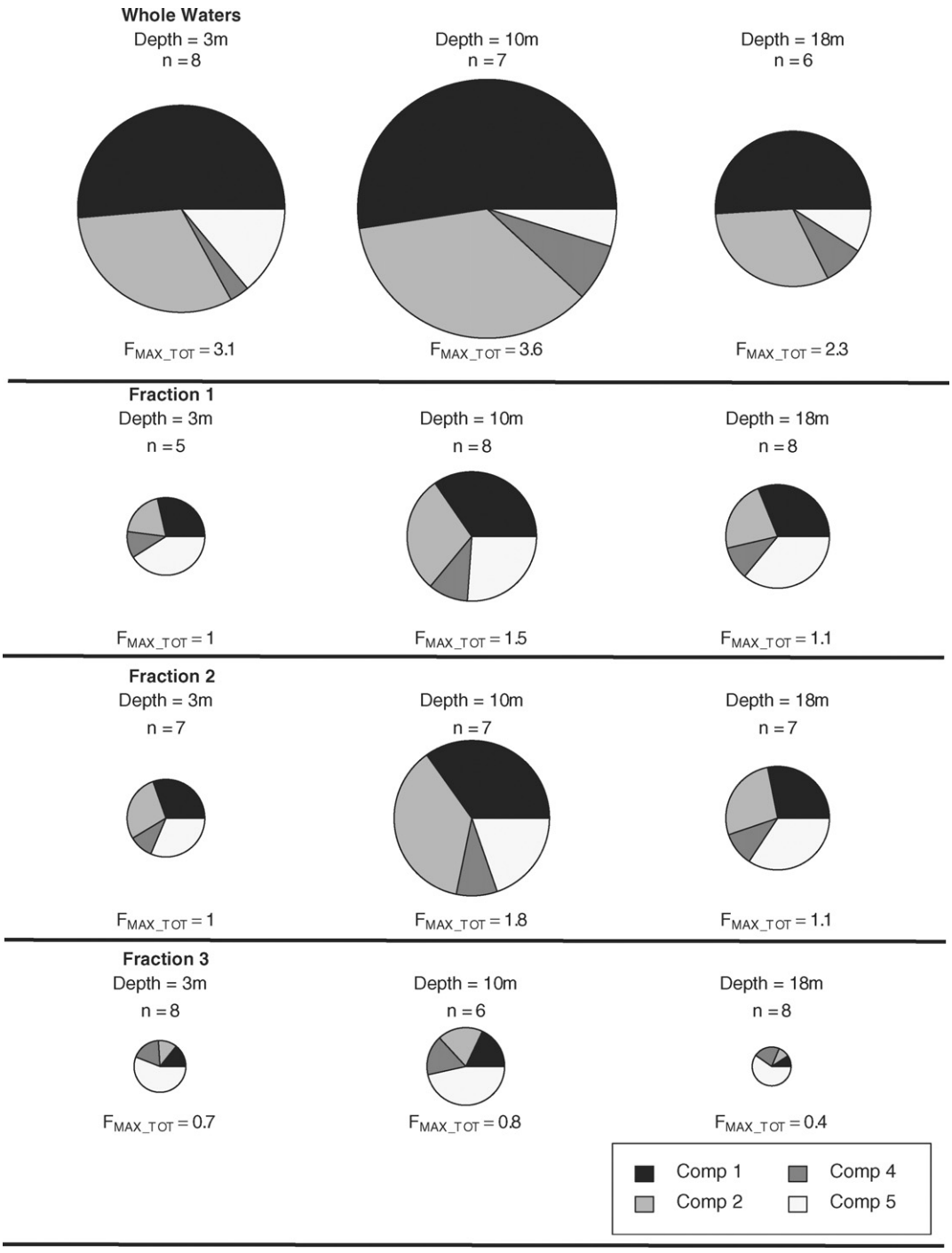

Fig. 5. Relative percent contribution of PARAFAC Components 1, 2, 4, and 5 for the whole waters and asymmetric flow-field flow fractionation generated fractions (Fractions 1–3) as a function of sample depth (3-, 10-, and 18-m). The diameter of pie charts was drawn proportional to the average total maximum fluorescence, F_{MAX_TOT}. The number of samples averaged, *n*, was appended to each pie chart.

The four PARAFAC component EEMs (Fig. 4, left-side panels) identified by the PARAFAC model have been previously identified by other researchers using PARAFAC or peak-picking methods. The ranges of the excitation and emission maxima for these components are summarized in Table 4. Components 1, 2, and 4 have primary and secondary excitation maxima and have been identified as humic-like fluorophores using PARAFAC and peak-picking methods. Component 5 only has a primary excitation maximum and has been identified as a protein-like fluorophore in a tidal estuary [50] and lake water [51].

Fluorescence maximum (F_{MAX}) values for Components 1, 2, 4, and 5 were plotted on a percent relative contribution basis in Fig. 5. Here, the diameters of the pie charts were drawn proportional to the average maximum total fluorescence, F_{MAX_TOT}. While the whole water samples had larger F_{MAX_TOT} values than the AF4-generated fractions, this result is not meaningful, as the fractions were diluted by the AF4 eluent. However, regardless of water fraction, F_{MAX_TOT} was highest for the 10-m samples, indicating stratification by depth of total fluorophores. Humic-like Components 1, 2, and 4 comprised the majority of the total fluores-

Table 4
Characteristics of the PARAFAC components.

PARAFAC component	Excitation maxima (nm)	Emission maxima (nm)	Description	Method	Sample source	Reference
1	225–245 (315–335)	405–430	Humic-like	PARAFAC	Estuary	[30]
			Humic-like	PARAFAC	Freshwater	[42]
2	247–267 (359–379)	455–485	Humic-like	PARAFAC	Estuary	[30]
4	374 (233)	465	Humic-like	Peak-picking	Treated wastewater	[7]
5	224–234	333–343	Protein-like	PARAFAC	Estuary	[50]
			Protein-like	PARAFAC	Lake water	[51]

Secondary maxima are shown in parentheses.

cence for the whole waters, Fraction 1, and Fraction 2. Conversely, Component 5 dominated Fraction 3, indicating this protein-like fluorophore was present in relatively large-sized DOM. Further, Component 5 was in least abundance for the 10-m depth samples for all water fractions, indicating stratification by depth of the type of fluorophores.

5. Conclusions

The physicochemical properties of CDOM at three depths in the Beaver Lake Reservoir (Lowell, AR) were studied between May and July 2010. BLW CDOM, as measured by AF4-UV_{254} and SUVA, showed that the 10-m depth samples had higher intensities and SUVA values than did the 3- and 18-m depth samples. For the 24 BLW CDOM samples, the diffusion coefficient peak maximums ranged from 3.5 to $2.8 \times 10^{-6}\,cm^2\,s^{-1}$, which corresponded to a molecular weight range of 680–1950 Da and a size of 1.6–2.5 nm. As such, the BLW CDOM was comprised of relatively low molecular weight aromatic carbon-containing molecules with no measured colloidal fraction (3000–100,000 Da). Fluorescence-PARAFAC modeling of the whole water samples and AF4-generated fractions yielded five principal components. However, Component 3 was attributed to instrument noise and discarded. PARAFAC Components 1, 2, and 4 had primary and secondary excitation maxima and resembled humic-like fluorophores identified previously by either PARAFAC or peak-picking techniques. Conversely, Component 5 had a single excitation maxima and was most similar to a protein-like fluorophore identified in estuarine and lake water samples. Samples from the 10-m sampling depth had the highest total fluorescence, echoing the AF4-UVA_{254} results, and adding further weight-of-evidence to the conclusion that the BLW CDOM was stratified by depth. Further, the relative percent contribution of each fluorophore varied by depth, indicating that the type of fluorophores were stratified by depth. The stratification of BLW CDOM shown here has potentially important implications for drinking water utilities that aim to reduce formation of disinfection byproducts.

Acknowledgements

The authors gratefully acknowledge the support of the Beaver Water District (Lowell, AR) for providing access for water sampling and funds to support DRM and operation of the laboratory equipment. Dr. Soheyl Tadjiki (Postnova Analytics, Salt Lake City, UT) provided invaluable analytical guidance for the operation of the AF4 system. Funds for the laboratory equipment and support of ADP and SLC were provided by the UA as part of the start-up package for JLF. Additional support of ADP was provided by the Doctoral Academy Fellowship program (UA).

Appendix A. Supplementary data

Supplementary data associated with this article can be found, in the online version, at doi:10.1016/j.chroma.2010.12.039.

References

[1] P.H. Santschi, K.A. Roberts, L. Guo, Environ. Sci. Technol. 36 (2002) 3711.
[2] M.W. LeChevallier, N.J. Welch, D.B. Smith, Appl. Environ. Microbiol. 62 (1996) 2201.
[3] J.J. Rook, Environ. Sci. Technol. 11 (1977) 478.
[4] A. Huguet, L. Vacher, S. Relexans, S. Saubusse, J.M. Froidefond, E. Parlanti, Org. Geochem. 40 (2009) 706.
[5] W.-H. Chu, N.-Y. Gao, Y. Deng, S.W. Krasner, Environ. Sci. Technol. 44 (2010) 3908.
[6] M. Kitis, T. Karanfil, A. Wigton, J.E. Kilduff, Water Res. 36 (2002) 3834.
[7] I.A.M. Worms, Z.A.G. Szigeti, S. Dubascoux, G. Lespes, J. Traber, L. Sigg, V.I. Slaveykova, Water Res. 44 (2010) 340.
[8] M. Kitis, T. Karanfil, J.E. Kilduff, A. Wigton, Water Sci. Technol. 43 (2001) 9.
[9] K.M. Cawley, J.A. Hakala, Y.P. Chin, Limnol. Oceanogr. Methods 7 (2009) 391.
[10] G. Yohannes, S.K. Wiedmer, M. Jussila, M.L. Riekkola, Chromatographia 61 (2005) 359.
[11] M. Baalousha, J.R. Lead, Environ. Sci. Technol. 41 (2007) 1111.
[12] S.A. Floge, M.L. Wells, Limnol. Oceanogr. 52 (2007) 32.
[13] S. Dubascoux, F. Von Der Kammer, I. Le Hecho, M.P. Gautier, G. Lespes, J. Chromatogr. A 1206 (2008) 160.
[14] E. Alasonati, V.I. Slaveykova, H. Gallard, J.P. Croue, M.F. Benedetti, Water Res. 44 (2010) 223.
[15] B. Stolpe, L.D. Guo, A.M. Shiller, M. Hassellov, Mar. Chem. 118 (2010) 119.
[16] T.N. Reszat, M.J. Hendry, Anal. Chem. 77 (2005) 4194.
[17] R. Krachler, R.F. Krachler, F. von der Kammer, A. Suephandag, F. Jirsa, S. Ayromlou, T. Hofmann, B.K. Keppler, Sci. Total Environ. 408 (2010) 2402.
[18] J. Boehme, M. Wells, Mar. Chem. 101 (2006) 95.
[19] X. Yang, C. Shang, W. Lee, P. Westerhoff, C.H. Fan, Water Res. 42 (2008) 2329.
[20] S.E. Cabaniss, Q.H. Zhou, P.A. Maurice, Y.P. Chin, G.R. Aiken, Environ. Sci. Technol. 34 (2000) 1103.
[21] T.C. Gadmar, R.D. Vogt, L. Evje, Int. J. Environ. Anal. Chem. 85 (2005) 365.
[22] S. Assemi, G. Newcombe, C. Hepplewhite, R. Beckett, Water Res. 38 (2004) 1467.
[23] M.E. Schimpf, K.D. Caldwell, J.C. Giddings (Eds.), Field-flow Fractionation Handbook, John Wiley & Sons, Inc., 2000.
[24] K.G. Wahlund, J.C. Giddings, Anal. Chem. 59 (1987) 1332.
[25] J.C. Giddings, Science 260 (1993) 1456.
[26] M. Baalousha, F.V.D. Kammer, M. Motelica-Heino, P. Le Coustumer, J. Chromatogr. A 1093 (2005) 156.
[27] H. Prestel, R. Niessner, U. Panne, Anal. Chem. 78 (2006) 6664.
[28] M.E. Schimpf, K.G. Wahlund, J. Microcolumn Sep. 9 (1997) 535.
[29] P.G. Coble, Mar. Chem. 51 (1996) 325.
[30] G.J. Hall, J.E. Kenny, Anal. Chim. Acta 581 (2007) 118.
[31] D.W. Johnstone, C.M. Miller, Environ. Eng. Sci. 26 (2009) 1163.
[32] C.M. Andersen, R. Bro, J. Chemometr. 17 (2003) 200.
[33] P.G. Coble, S.A. Green, N.V. Blough, R.B. Gagosian, Nature 348 (1990) 432.
[34] G.V. Korshin, M.M. Benjamin, H.S. Chang, H. Gallard, Environ. Sci. Technol. 41 (2007) 2776.
[35] D.W. Johnstone, N.P. Sanchez, C.M. Miller, Environ. Eng. Sci. 26 (2009) 1551.
[36] B. Hua, K. Veum, J. Yang, J. Jones, B.L. Deng, Environ. Monit. Assess. 161 (2010) 71.
[37] C.A. Stedmon, R. Bro, Limnol. Oceanogr. Methods 6 (2008) 572.
[38] S. Sen, B.E. Haggard, I. Chaubey, K.R. Brye, T.A. Costello, M.D. Matlock, Water Air Soil Pollut. 179 (2007) 67.
[39] A.D. Eaton, L.S. Clesceri, E.W. Rice, A.E. Greenberg (Eds.), Standard Methods for the Examination of Water & Wastewater, American Public Health Association, Washington, DC, 2005.
[40] A. Chatterjee, J. Am. Chem. Soc. 86 (1964) 3640.
[41] R.G. Zepp, W.M. Sheldon, M.A. Moran, Mar. Chem. 89 (2004) 15.
[42] C.A. Stedmon, S. Markager, Limnol. Oceanogr. 50 (2005) 686.

[43] J.B. Fellman, D.V. D'Amore, E. Hood, R.D. Boone, Biogeochemistry 88 (2008) 169.
[44] K.J. Howe, M.M. Clark, Environ. Sci. Technol. 36 (2002) 3571.
[45] J.L. Weishaar, G.R. Aiken, B.A. Bergamaschi, M.S. Fram, R. Fujii, K. Mopper, Environ. Sci. Technol. 37 (2003) 4702.
[46] R. Beckett, Z. Jue, J.C. Giddings, Environ. Sci. Technol. 21 (1987) 289.
[47] P.J.M. Dycus, K.D. Healy, G.K. Stearman, M.J.M. Wells, Sep. Sci. Technol. 30 (1995) 1435.
[48] M. van Bruijnsvoort, R. Tijssen, W.T. Kok, J. Polym. Sci. Pol. Phys. 39 (2001) 1756.
[49] J. Moon, S.H. Kim, J. Cho, Colloid Surf. A: Physicochem. Eng. Aspects 287 (2006) 232.
[50] G.J. Hall, K.E. Clow, J.E. Kenny, Environ. Sci. Technol. 39 (2005) 7560.
[51] B. Hua, F. Dolan, C. McGhee, T.E. Clevenger, B. Deng, Int. J. Environ. Anal. Chem. 87 (2007) 135.
[52] J.R. Lead, E. Balnois, M. Hosse, R. Menghetti, K.J. Wilkinson, Environment Int. 25 (1999) 245.
[53] J.R. Lead, K.J. Wilkinson, E. Balnois, B.J. Cutak, C.K. Larive, S. Assemi, R. Beckett, Environ. Sci. Technol. 34 (2000) 3508.
[54] N. Park, J. Cho, J. Membrane Sci. 315 (2008) 133.